*Revista Mexicana de Astronomía y Astrofísica*, **57**, 433–444 (2021)

https://doi.org/10.22201/ia.01851101p.2021.57.02.15

# INTERPRETATION OF OPTICAL AND IR LIGHT CURVES FOR TRANSITIONAL DISK CANDIDATES IN NGC 2264 USING THE EXTINCTED STELLAR RADIATION AND THE EMISSION OF OPTICALLY THIN DUST INSIDE THE HOLE

E. Nagel[1], F. Gutiérrez-Canales[1], S. Morales-Gutiérrez[1], and A. P. Sousa[2]

*Received May 10 2021; accepted August 6 2021*

ABSTRACT

In the stellar forming region NGC 2264 there are objects catalogued as hosting a transitional disk according to spectrum modeling. Four members of this set have optical and infrared light curves coming from the *CoRoT* and *Spitzer* telescopes. In this work, we try to simultaneously explain the light curves using the extinction of the stellar radiation and the emission of the dust inside the hole of a transitional disk. For the object Mon-296, we were successful. However, for Mon-314, and Mon-433 our evidence suggests that they host a pre-transitional disk. For Mon-1308 a new spectrum fitting using the 3D radiative transfer code Hyperion allows us to conclude that this object hosts a full disk instead of a transitional disk. This is in accord to previous work on Mon-1308 and with the fact that we cannot find a fit for the light curves using only the contribution of the dust inside the hole of a transitional disk.

RESUMEN

En la región de formación estelar NGC 2264 se encuentran objetos catalogados como anfitriones de discos transicionales según los modelos del espectro. Para cuatro de sus miembros se tienen curvas de luz en el óptico y en el infrarrojo provenientes de los telescopios CoRot y Spitzer. Tratamos de explicar ambas curvas de luz simultáneamente usando la extinción de la radiación estelar y la emisión del polvo dentro del agujero de un disco transicional. Para el objeto Mon-296 fuimos exitosos pero nuestra evidencia indica un disco pre-transicional para Mon-314 y Mon-433. Un nuevo ajuste del espectro con el código 3D de transferencia radiativa Hyperion nos permite concluir que Mon-1308 tiene un disco completo en lugar de un disco transicional. Esto coincide con trabajo previo sobre Mon-138 y con el hecho de no haber encontrado un ajuste de las curvas de luz a partir del uso exclusivo de la contribución del polvo dentro del agujero de un disco transicional.

*Key Words:* dust, extinction — protoplanetary disks — stars: pre-main-sequence



## 1. INTRODUCTION

Spectral and photometric variability of young stellar objects (YSOs) is the usual outcome of multiwavelength campaigns (Stauffer et al. 2014, 2015, 2016; Cody et al. 2014; Morales-Calderón et al. 2011). For young stars in NGC 2264, Stauffer et al. (2014) extract the accretion burst dominated light curves (lcs), Stauffer et al. (2015) show the short-duration periodic flux dips in the lcs and Stauffer et al. (2016) present the stochastically varying lcs. Cody et al. (2014) extract optical and infrared (IR) lcs from the *Spitzer* and *CoRoT* telescopes for 162 classical T Tauri stars (CTTSs) where flux variations are clearly detected. They catalog them into seven distinct classes describing multiple origins of young star variability: circumstellar obscuration events, hot spots, accretion bursts and structural changes in the inner disk. Focusing at 3.6 and 4.5$\mu$m, lcs of hundreds

[1]Departamento de Astronomía, Universidad de Guanajuato, México.
[2]Institut de Planétologie et d'Astrophysique de Grenoble, Université Grenoble Alpes, France.

of objects in the Orion Nebula Cluster, Morales-Calderón et al. (2011) found variability that can be interpreted by processes occurring in the disk, like density structures intermittently blocking our line of sight. From this and other studies is extracted the label "dippers" for the objects showing changes in the flux that can be explained by circumstellar material crossing the line of sight directed towards the object. Bouvier et al. (1999) refer to the prototypical dipper AA Tau interpreting the lcs by asymmetries at the inner edge of the dusty disk where a magnetically induced warp is formed. This object showed a sudden dimming in 2011 that can be interpreted as the extinction produced by an overdense region orbiting around the star (Bouvier et al. 2013). Alencar et al. (2010) use observations of the *CoRoT* telescope to search for AA Tau type like objects in NGC 2264. They conclude that the dipper objects are common because the frequency is $\approx 30$ to 40% in YSOs with dusty disks.

Identification of dippers (Rodriguez et al. 2017) and its interpretation locating material in the innermost regions of the disk (Bodman et al. 2017; Nagel & Bouvier 2020) is a key issue to characterize the interaction of the magnetosphere and the disk. We need a reasonable amount of material in the accretion streams to account for the dipper behavior (Bodman et al. 2017). However, the weak accretion signatures of the transitional disks (TDs) in the sample of dippers in Ansdell et al. (2016) is enough to interpret the variability of the lcs with the extinction of the material in the innermost part of the disk, which is interacting with the magnetospheric lines.

Ansdell et al. (2016) interpret the lcs of the ten objects in their sample using three different mechanisms: occulting inner disk warps, vortices caused by the Rossby wave instability (RWI) and transiting circumstellar clumps. Warps require the presence of material in the innermost region of the circumstellar environment, which is revealed by strong accretion signatures. The RWI is responsible for forming non-axisymmetric structures (Lovelace & Romanova 2014) as vortices (Meheut et al. 2010), which explain shallow, short-duration and periodic dippers in the Ansdell et al. (2016)'sample. Transiting circumstellar clumps can explain the lc of the evolved disk in EPIC 205519771 because the lc is aperiodic and the accretion signatures are weak. The few days timescale for the variations in any of these objects leads to assume that any mechanism requires material in the innermost circumstellar zones. The interpretation of lcs with low periodicity indicates that the explanation should include the effects of the highly dynamic environment close to the star. For different campaigns, in a subsample of dippers studied by McGinnis et al. (2015) there is a change between unstable and stable accretion regimes (Blinova et al. 2016), affecting the mass accretion rate towards the star, $\dot{M}$ (Kulkarni & Romanova 2008), and in this way shaping the behavior of the lcs.

The concept of pre-transitional (PTDs) and TDs has a recent presence in the discussion of YSOs. Using sub-millimeter observations, Andrews et al. (2011a) observed 12 TDs with cavities in the range from 15 to 73 AU. Espaillat et al. (2010, 2011) favor its existence modeling the SEDs including the presence of an inner disk component and emission of dust coming from the gap or hole. From this modeling, Espaillat et al. (2010) catalogued LkCa 15, UX TauA, and ROX44 as hosting PTDs, but GM Aur and DM Taos hosting TDs. The modeling requires some optically thin dust in the hole of the disk associated for GM Aur but for DM Tau the hole is empty of grains, as previously interpreted by Calvet et al. (2005). The variability of PTDs is interpreted in the sample of Espaillat et al. (2011) by changes of $\approx 20\%$ in the inner disk wall height which they associate to a warp. For the TD in GM Aur, the variability between two campaigns is explained by changes in the inner edge height of the disk at 23 AU from 2.9 to 3.2 AU. The absence of variability for DM Tau is interpreted using the absence of dust within the hole of its TD as an argument to justify the non-existence of a mechanism to explain the variability occurring at this timescale. For GM Aur, the model by Ingleby et al. (2015) requires changes in $\dot{M}$ associated to inhomogeneities in the inner disk as the process explaining ultraviolet, optical and near-infrared (near-IR) observations. Nagel et al. (2017) also model this object, but using the intermittent formation of a sublimation wall associated to accumulation of matter as the physical mechanism to explain variability in the SpeX spectrum. Both analyses point out the multiplicity of ways to explain this kind of objects but restrict the structures formed in the inner region as the relevant aspect to focus on.

In YSOs, one way to interpret optical and infrared lcs is by means of the dust in the disks surrounding them. In many cases, along with the lcs, their spectral energy distributions (SEDs) are the only sources of information for them; thus, when images are not available, the physical characteristics of these systems should be only interpreted by modeling their fluxes, or using selection criteria defined by different ranges in some phometric colors and spec-

tral indices (Fang et al. 2009; Merín et al. 2010; Cieza et al. 2010; Muzerolle et al. 2010).

Help to choose an adequate structure around each object comes from the distinction between a full and a TD shown as a different signature in the SED but also its effect on the optical lc. During the last years, using the available new facilities, images of TDs are obtained for a few systems. These images show that the structure is complex, presenting vortices and spirals as in the TD HD 135344B (Muto et al. 2012; van der Marel et al. 2016) with a bias towards large cavities (van der Marel et al. 2018). The formation of spirals is justified with a spiral density wave theory in Muto et al. (2012). Note that the stellar radiation produces a puffed up inner rim that occults some disk regions from this radiation, clearly changing the radial temperature profile and affecting the formation of structures (Dullemond & Monnier 2010). Flaherty et al. (2012) explain the observed variability in the IR range with changes in the inner disk structure, i.e. scale height fluctuations. We summarize this by saying that a physically correct model should be able to explain many sources of information: photometry, spectra and images. These ideas highlight the importance of being able to identify which kind of disk we are dealing with. However, due to the difficulty to achieve enough spatial resolution to obtain images for many of the objects, even in close stellar forming regions, the interpretation leads to degeneracy; thus at most we can find models consistent with the observations.

In this work, we focus on TDs; the interpretation of the information coming from the *Spitzer Space Telescope* and other facilities allows the astronomy community to be confident that TDs are out there (Espaillat et al. 2007, 2008, 2014). Surveys of objects allow a characterization; for instance, the observed $\dot{M}$ estimated using the UV excesses caused by the magnetospheric streams falling towards the stellar surface can be explained when these estimates are compared with the value for $\dot{M}$ of classical T Tauri stars (Najita et al. 2007, 2015). The disk mass ($M_{\rm d}$) is correlated with $\dot{M}$ either in full disks (Manara et al. 2016) or in TDs (Owen & Clarke 2012; Najita et al. 2015). This lead us to conclude that an estimated $\dot{M}$ using detected UV excesses in TDs is a key piece of information to guarantee the presence of gas in the hole (Manara et al. 2014). The dust attached to it is responsible to shape lcs by extinction of the stellar radiation. The analysis of lcs by Ansdell et al. (2016) point out occulting inner disk warps and transiting circumstellar clumps as possible processes explaining the observations. For the TD candidates analyzed in our work, a non-zero $\dot{M}$ guarantees that there is gas in the inner region of the disk. Assuming that the dust is attached to the gas, the previous mechanism, or any other that uses dust in the innermost region of the disk either as optically thin inside the cavity in a TD or as an optically thick dusty ring in the PTD case, are plausible scenarios to explain the lcs.

It is usually assumed that the star is not variable in the timescale of the physical processes included to model the lc variability, such that the asymmetry of the dust distribution leads to the features observed. The main contributor to the optical emission is the star. This means that the depth of the signal in the optical lc is given by the amount of dust eclipsing the star. A reservoir of optically thin dust prone to extinct the star is found in the inner hole of TDs.

Specifically, we focus on the sample of TD candidates in the NGC 2264 stellar forming region presented in Sousa et al. (2019). From this sample we choose the objects that have contemporaneous optical and infrared (IR) lcs from *CoRoT* and *Spitzer*, respectively (McGinnis et al. 2015), in order to check the effect on the lcs caused by the material in the disk hole. These objects are Mon-296, Mon-314, Mon-433 and Mon-1308. We focus the study on the YSO Mon-1308 because for this system, we have two different scenarios proposed. The first one is analysed in Nagel & Bouvier (2019) where they simultaneously explain *CoRoT* and *Spitzer* lcs using a full disk as the optically thick structure responsible for the shape of the optical lc, because it occults sections of the stellar surface; also, it is responsible for the shape of the IR lc using the disk emission. The second one is presented in Sousa et al. (2019) where they modeled the SED of a sample of objects using 3 possible cases: a full disk, no disk, and a TD. For Mon-1308, their best fit is a TD with a 20.18 AU hole, which is completely different from the full disk structure required in Nagel & Bouvier (2019). The aim of this work is to complement the analysis in Nagel & Bouvier (2019), which searched for an explanation of the optical and IR lcs of Mon-1308 using a full disk; instead, we extend the analysis using a TD.

As a complementary analysis, we repeat the steps applied to Mon-1308 for the other 3 TD candidates that also share contemporaneous IR and optical lcs. From the whole set, we point out differences in the tuning of the modeling required to look for the interpretation of the lcs of systems that have a range of hole sizes spanning from 0.12 AU to 20.18 AU. In the analysis, we should not forget that not all the lcs are

TABLE 1

OBSERVED PARAMETERS

| Object | $R_\star(R_\odot)$ | $M_\star(M_\odot)$ | $T_\star$( K) | $\dot{M}_{\rm min}$[a] | $\dot{M}_{\rm obs}$[a] | $\dot{M}_{\rm max}$[a] | $R_{\rm H}$(AU) |
|---|---|---|---|---|---|---|---|
| Mon-296 | 1.71 | 1.42 | 4950 | | 1.73 | | 0.12 |
| Mon-314 | 1.35 | 0.29 | 3360 | 5.75 | 5.75 | 13.5 | 3.58 |
| Mon-433 | 0.99 | 0.44 | 3680 | 1.38 | 2.04 | 2.51 | 7.39 |
| Mon-1308 | 1.59 | 0.63 | 3920 | 5.62 | 8.51 | 28.8 | 20.18 |

[a]All the $\dot{M}$ are given in units of $10^{-9}\,M_\odot{\rm yr}^{-1}$.

TABLE 2

*COROT* LIGHT CURVES PERIODS FOR THE 2008 AND 2011 CAMPAIGN

| Object | P(days), 2008 campaign | P(days), 2011 campaign |
|---|---|---|
| Mon-296 | 2.51 | 3.91 |
| Mon-314 | — | 3.38 |
| Mon-433 | — | — |
| Mon-1308 | 6.45 | 6.68 |

periodic and not always there is a high resemblance between the IR and the optical lcs.

In § 2 we present the details of the sample studied; in § 3 the model is explained, in § 4 the modeled lc for the 4 objects studied is presented and finally, in § 5 and § 6, the discussion and conclusions are shown.

## 2. SAMPLE OF OBJECTS STUDIED

The objects studied belong to the sample of McGinnis et al. (2015) for objects having AA-Tau like and variable extinction dominated lcs and to the sample of TD candidates in Sousa et al. (2019). The hypothesis for this set of objects is that the dust inside the hole is relevant to explain both the lcs in the optical and in the IR. The objects are: Mon-296, Mon-314, Mon-433, and Mon-1308. The hole size $R_{\rm H}$, the stellar mass $M_\star$, the stellar radius $R_\star$, the stellar temperature $T_\star$, the minimum $\dot{M}_{\rm min}$, the maximum $\dot{M}_{\rm max}$ and the observed disk mass accretion rate $\dot{M}_{\rm obs}$ are presented in Table 1; unless otherwise mentioned, these parameters come from Venuti et al. (2014). The mass accretion rate comes from two estimates: ($u$-$g$) and ($u$-$r$) color excesses modeling. $\dot{M}_{\rm obs}$ is taken from the first estimate. $\dot{M}_{\rm min}$ and $\dot{M}_{\rm max}$ are the minimum and maximum values from both estimates, including the errors. Notice that the range of $R_H$ spans from 0.12 AU in Mon-296 to 20.18 AU in Mon-1308, a difference of more than two orders of magnitude, allowing to analyse the effect of this parameter in the lcs.

The analysis of the periodicity of the lcs for the objects in the sample was done by Cody et al. (2014) using as a starting point the auto correlation function (ACF) defined and used to calculate the rotational period for a sample of M dwarfs by McQuillan et al. (2013). Applied to a time series, the maximum of the ACF gives the time elapsed between two points for which the signal is the most correlated. In order to confirm that the selected period really corresponds to the main period of the data, Cody et al. (2014) compute a Fourier transform periodogram and search for peaks within 15% of the frequency associated to the period obtained. From this analysis, the objects in our sample show the periods given in Table 2.

Two of the systems show a clear periodicity in their *CoRoT* lcs (Mon-296, Mon-1308). A structure explaining this can be a fixed warp in the inner section of the disk that is repeated periodically along the line of sight. The lc for Mon-314 has a low-probability periodicity in the 2011 epoch and is non periodic in the 2008 epoch, which indicates that the physical mechanism shaping the lc is not long-lived. Thus, a warp may or may not be the cause to explain the 2011 epoch lc. For Mon-433, both epochs the lc is not periodic. Thus, the shape cannot be described with a stable warp. However, looking at the lc, there is a clear sequence of peaks and valleys, such that the occulting structures are locally periodic (they are moving at the Keplerian velocity according to their location) but the dominant one is not always the same, meaning that the period is changing. Also from the lc we can conclude that the timescale of the variability is a few days, indicating that the structures are located close to the inner edge of the disk. The shaping of this region is given by the interaction of the disk with the stellar magnetic

TABLE 3

OBSERVED AMPLITUDES FOR THE LCS

| Object | $\Delta mag_{\rm obs}$[a] | $\Delta mag_{\rm IR,obs}$[b] |
|---|---|---|
| Mon-296 | $0.2-0.7$ | $<0.1$ |
| Mon-314 | $0.1-0.15$ | $0.1-0.15$ |
| Mon-433 | $0.2-0.4$ | $0.2-0.4$ |
| Mon-1308 | $0.2-0.4$ | $0.2-0.4$ |

[a]Values from the *CoRoT* Telescope.

[b]Values from the *Spitzer* Telescope.



field lines (Romanova et al. 2013; Nagel & Bouvier 2020).

Another aspect to be pointed out is the resemblance or not of the *CoRoT* and *Spitzer* lcs: for Mon-296 both lcs are completely different, for Mon-314 and Mon-433 there is a resemblance between both lcs and, finally, for Mon-1308, the resemblance is remarkable. A high resemblance between the lcs suggests a strong connection between the mechanisms explaining them.

The observational values that we aim to model are the amplitudes for the optical ($\Delta mag_{obs}$) and the IR lcs ($\Delta mag_{\rm IR,obs}$). These values are given in data of the *CoRoT* and *Spitzer* telescopes extracted by McGinnis et al. (2015) and included in Table 3. $\Delta mag_{\rm obs}$ from the *CoRoT* Telescope and $\Delta mag_{\rm IR,obs}$ are taken from the *Spitzer* telescope. The *Spitzer* photometric data include values for wavelengths of 3.6 and 4.5$\mu$m. Because the behavior is similar in both wavelengths we choose 3.6$\mu$m for the analysis.

## 3. MODELING

For the modeling of the optical lc for each object, we modify the code used in Nagel & Bouvier (2019) to include the extinction by dust in a disk hole where the contribution of an optically thick region is neglected. We include also the emission of the dust located in the hole in order to consistently calculate the modeled IR lc. As mentioned, the lcs are completely shaped by the spatial dust distribution which is given by the gas density; the gas (and dust) is inwards limited by the magnetospheric radius, $R_{\rm mag}$, which is assumed to equal the Keplerian radius ($R_{\rm k}$) at the period extracted from the optical lcs and outwards limited by the hole radius ($R_{\rm H}$) given in Sousa et al. (2019). The optically thin material is distributed according to the gas density $\rho$, which depends on the azimuthal angle $\phi$ and the vertical coordinate $z$, and is given by

$$\rho = A\cos(\frac{\phi-\phi_0}{2})e^{-z/H_H}(1-\beta\frac{R}{R_H}), \qquad (1)$$

where $\phi=\phi_0$ is the location where the maximum density is found and the factor 1/2 allows to have only one maximum in the $\phi$ range. The value for $\phi_0$ is chosen such that at $phase=0.5$ (center of the plotted lc) the maximum density (and the minimum optical flux) is located along a line of sight towards the star. This density peak is responsible for periodically occulting the star, as required to interpret the optical lc. The argument inside the exponential simply models a natural concentration tendency towards the midplane of the disk. We do not assume that the hole material has reached vertical hydrostatic equilibrium. The scale height $H_{\rm H}$ represents a width of the accreting stream in the hole, which we fix as $H_{\rm H}=0.1R_{\rm H}$, a value typical of the disk scale height at the location where the material "falls" to the hole from a stationary disk in vertical hydrostatic equilibrium. Because the velocity in the stream is much larger than the accreting velocity in the disk, the density in the hole is lower, as required to get an optically thin environment. As the timescales between disk and hole are different, it is safe to assume that in the hole, the vertical equilibrium is not reached. In any case, the exact shape of the functional form of $\rho$ is irrelevant to the main conclusions presented in this work, because the amplitude of the optical lc is mainly given by the density maximum, whose order of magnitude is given by $\dot{M}$ and not by the functional form of $\rho$.

The free parameter $\beta$ models the radial concentration of dust/gas: $\beta=0$ corresponds to a homogeneous distribution, and $\beta=1$ indicates that the material is concentrated towards the inner edge of the hole. Note that this latter case is close to what one expects for a structure moving at the observed periodicity ($3-10$ days) for the sample of objects, where $R_k$ is located in the inner region. We do not include a detailed analysis of dust sublimation. Even for the $\beta=1$ case, most of the region responsible to shape the lcs is beyond the magnetospheric radius, which is the lower limit for the grid used. The constant coefficient $A$ is calculated assuming two facts; first, that all the material being incorporated into the hole (at $R_H$) arrives at the star in the free-fall time given by $t_{\rm ff}=\frac{R_{\rm H}}{v_{\rm ff}}$ where

$$v_{\rm ff}=\sqrt{\frac{2GM_\star}{R_\star}}\sqrt{1-\frac{R_\star}{R_{\rm H}}} \qquad (2)$$

is the free-fall velocity; second, that $\dot{M}$ resulting of this process is equal to the observed value, $\dot{M}_{\rm obs}$.

Note that the dust located in the gas distributed as in equation 1 is responsible to shape the IR lc. In fully optically thin stellar surroundings, the IR photometric variability is small because the dust grain emission is not extincted or blocked. However, in the system configuration there are grains occulted behind the star. For Mon-296, whose hole is small, the fractional area representing this occultation ($f_{\rm A} = \frac{\pi R_\star^2}{\pi R_{\rm H}^2 \cos i}$) amounts to 0.009 such that the blocking of this fraction of the emission corresponds to $\Delta mag_{\rm IR} \approx -2.5 \log 10(1 - f_{\rm A}) \approx 0.01$, which is of the order of magnitude of $\Delta mag_{\rm IR,obs}$, as can be seen in Table 3. For Mon-314,433 and 1308 the variability coming from this geometrical occultation is 3 to 4 orders of magnitude smaller than for Mon-296. This means that for the 3 objects the dust extinction is relevant to search for a physical configuration to explain $\Delta mag_{\rm IR,obs}$.

We assume that all the material in the hole is moving at the same rotational velocity. However, this is not true. The expected orbit for each accreting particle is a spiral, because at $R_{\rm H}$ and $R_{\rm k}$ the orbital Keplerian periods in a circular trajectory are $\approx$ 4000 days and 6.45 days, respectively, which can be compared to $t_{\rm ff} = 89$ days, where the parameters for Mon-1308 are used. In other words, during the free-fall, the particle orbits several times around the star before it arrives at the surface. The assumption of a dynamical model will locally change the dust distribution, but to fit $\Delta mag_{\rm obs}$ the most important parameter is the maximum surface density along the line of sight. The maximum is calculated using $\rho$, and this latter will not change appreciably using a detailed model.

## 4. RESULTS

The fitting of $\Delta mag_{\rm obs}$ and $\Delta mag_{\rm IR,obs}$ is done using two free parameters: $\beta$ and the dust to gas ratio $\zeta$. The latter is parameterized by $\alpha$ where $\zeta = \alpha \zeta_{\rm typ}$ and $\zeta_{\rm typ} = 0.01$ is assumed as typical for protoplanetary disks. According to the model, the value $\beta = 1$ corresponds to the configuration with the largest concentration of material close to the star which, as mentioned in § 3, is a physically expected configuration. For this reason, the fiducial model is defined by $\alpha = 1$ and $\beta = 1$.

For each object, $\dot{M}_{\rm obs}$ is given as in Table 1 and $H_H$ is fixed to $H_{\rm H} = 0.1 R_{\rm H}$. We note that there is a degeneracy between $\dot{M}$ and $\zeta$ because if both parameters increase/decrease then the amount of dust increases/decreases keeping the shape of the spatial distribution of material. We decided to fix $\dot{M}$ at $\dot{M}_{\rm obs}$ because it is consistent with the estimates based on observations, and therefore we interpret the model according to changes in $\zeta$ ($\alpha$). The value for $\Delta mag_{\rm IR}$ is assigned to the maximum magnitude change for the 3.6$\mu$m *Spitzer* band. Note that the behavior for the 4.5$\mu$m band is similar, as can be seen in the *Spitzer* observations shown in McGinnis et al. (2015) for the set of objects studied here.

We find models consistent with the observed range of $\Delta mag_{\rm obs}$ and $\Delta mag_{\rm IR,obs}$ using a grid in the ranges of $\alpha$ and $\beta$ given by $[0.1, 10]$ and $[0, 1]$, respectively. In Table 4, we present the parameters for the representative consistent models found in § 4.1,§ 4.2,§ 4.3, and § 4.4. The first column corresponds to the object name, the second column to $\alpha$, and the third to $\beta$. The next three columns are associated to the optical lc; the minimum flux of the star, $F_{\rm min,opt}$, the maximum flux of the star, $F_{\rm max,opt}$ and $\Delta mag$. The final three columns are associated to the IR lc; the minimum total flux of the star plus disk, $F_{\rm min,IR}$, the maximum total flux of star plus disk, $F_{\rm max,IR}$ and $\Delta mag_{\rm IR}$. All the fluxes are given in units of $10^{-12}\,{\rm erg\,cm^{-2}\,s^{-1}}$.

### 4.1. *Mon-1308*

For both $\Delta mag_{\rm obs}$ and $\Delta mag_{\rm IR,obs}$ the range is $[0.2, 0.4]$. A fit for $\Delta mag_{\rm obs}$ is found when $\alpha = 5$ (with $0.8 < \beta < 1$), $\alpha = 7$ (with $0 < \beta < 1$) and $\alpha = 10$ (with $0 < \beta < 0.8$). Due to the grid of models, we run models for $\alpha = 5, 7$ and 10 but not for intermediate values; however other models with values of $\alpha$ between 5 and 10 are also inside the range for $\Delta mag_{\rm obs}$. For these models $\Delta mag_{\rm IR} < 10^{-4}$ which is 3 orders of magnitude lower than required for a reasonable fit. The parameters for the models with $\beta = 1$ are shown in Table 4.

In order to favor these models, either the dust to gas mass ratio should be higher than expected in a typical disk, or $\dot{M}$ should be outside the observational estimates. In any case, even if this can be achieved, only $\Delta mag_{\rm obs}$ can be explained; the fitting of $\Delta mag_{\rm IR,obs}$ is left to another physical mechanism.

IR photometric variability is not expected in an optically thin stationary system because all the emitting material contributes to the IR lc. However, this is not true if there is extinction and occultation; namely the dust extincts and the star occults the dust behind it. Including both mechanisms, the model variability in the IR is small compared to the one in the optical. The previous result, and the fact that for Mon-1308, $\Delta mag_{\rm obs} \approx \Delta mag_{\rm IR,obs}$, explains

TABLE 4

PARAMETERS FOR REPRESENTATIVE MODELS

| Object | $\alpha$ | $\beta$ | $F^a_{\rm min,opt}$ | $F^a_{\rm max,opt}$ | $\Delta mag$ | $F^a_{\rm min,IR}$ | $F^a_{\rm max,IR}$ | $\Delta mag_{\rm IR}$ |
|---|---|---|---|---|---|---|---|---|
| Mon-296 | 1 | 1 | 47.7 | 57.6 | 0.226 | 5.30 | 5.35 | $1.05 \times 10^{-2}$ |
| Mon-296 | 10 | 0.5 | 30.3 | 55.0 | 0.719 | 8.01 | 8.33 | $4.37 \times 10^{-2}$ |
| Mon-314 | 0.5 | 0.7 | 3.267 | 3.60 | 0.107 | 1.610 | 1.619 | $5.68 \times 10^{-3}$ |
| Mon-314 | 0.7 | 1 | 3.265 | 3.60 | 0.107 | 1.612 | 1.620 | $5.58 \times 10^{-3}$ |
| Mon-433 | — | — | — | — | — | — | — | — |
| Mon-433 | — | — | — | — | — | — | — | — |
| Mon-1308 | 5 | 1 | 10.8 | 14.1 | 0.284 | 2.94800 | 2.94812 | $4.29 \times 10^{-5}$ |
| Mon-1308 | 7 | 1 | 9.79 | 14.1 | 0.398 | 2.94803 | 2.94819 | $5.98 \times 10^{-5}$ |

[a]All the fluxes are given in units of $10^{-12}\,{\rm erg\,cm^{-2}\,s^{-1}}$.



our inability to consistently model IR and optical lcs using optically thin material in the hole of a TD.

The last analysis leads us to conclude that instead of a TD, a possible configuration to simultaneously explain both the optical and the IR lcs is a PTD. In spite of the classification of Sung et al. (2009) where Mon-1308 is catalogued as a TD due to the amount of dust in the inner disk, we try to interpret this object as a PTD. For the modeling of Mon-1308 in Nagel & Bouvier (2019) required an optically thick warp located at $R_{\rm mag}$, meaning that the remaining emission should be associated to the disk outside the warp. Nagel & Bouvier (2019) do not explicitly characterize the shape of the disk but in accordance with the analysis given here, the thick warp plays the role of the inner disk of the PTD.

Taken together, the previous discussion should be connected to the SED fitting code used in Sousa et al. (2019) which only includes the dust emission outside an empty hole. In the model presented here, the dust emission should come from an optically thin hole and the outer disk. We point out that in our model the variability is completely associated to the dust distribution inside the hole. In the case of a PTD, the observed emission should be interpreted as coming from both an inner, an outer disk, and the dusty gap. A follow-up goal is to find a SED fit consistent with the model described in Nagel & Bouvier (2019), where the innermost structure is a sublimation wall covering a small radial range.

The optical flux from our TD model lies between the $F_{\rm min,opt}$ and $F_{\rm max,opt}$ values given in Table 4. These values are consistent with the SED fitting in Nagel & Bouvier (2019). For Mon-1308, the model presented in Nagel & Bouvier (2019) shows that the flux at 4.5$\mu$m coming from the full disk, namely $F_{\rm disk,4.5}$ is similar to the flux at 4.5$\mu$m coming from the star, namely $F_{\star,4.5}$ which is around half the observed flux, namely $F_{\rm obs,4.5}$. In Table 4 the range of fluxes modeled at 3.6$\mu$m is presented, lying between the values $F_{\rm min,IR}$ and $F_{\rm max,IR}$. These values are consistent with $F_{\rm disk,4.5}+F_{\star,4.5}$. In the model by Sousa et al. (2019), $F_{\star,4.5} \approx F_{\rm obs,4.5}$, because there is a negligible contribution of any part of the disk. We note that in their model, $T_\star$ (a free parameter) is 1091 K higher than the values estimated in Venuti et al. (2014), allowing us to suggest that a new model including an inner disk and a star with a lower $T_\star$ as the main contributors in the near-IR is reasonable. Besides, note that in McGinnis et al. (2015), $F_{\rm disk,4.5}/F_{\star,4.5} = 0.7$ meaning that there is a clear contribution of material around the star. This suggests that PTD or full disks are configurations likely to explain this excess.

In order to pursue this further, we find a new synthetic SED using the Python-based fitting code Sedfitter (Robitaille 2017) based on the 3D dust continuum radiative transfer code Hyperion, an open-source parallelized three-dimensional dust continuum radiative transfer code by Robitaille (2011), which was used for the modeling in Sousa et al. (2019). This code is composed of modular sets with components that can include a stellar photosphere, a disk, an envelope, and ambipolar cavities. For Mon-1308, we used two sets of models. Model 1 is composed of a stellar photosphere and a passive disk, Model 2 includes a stellar photosphere, a passive disk, and a possible inner hole. The Hyperion SED model includes only a passive disk, and does not consider disk heating due to accretion. The input parameters of the Hyperion Sedfitter are a range of $Av$, the distance from the Sun, the fluxes, and the

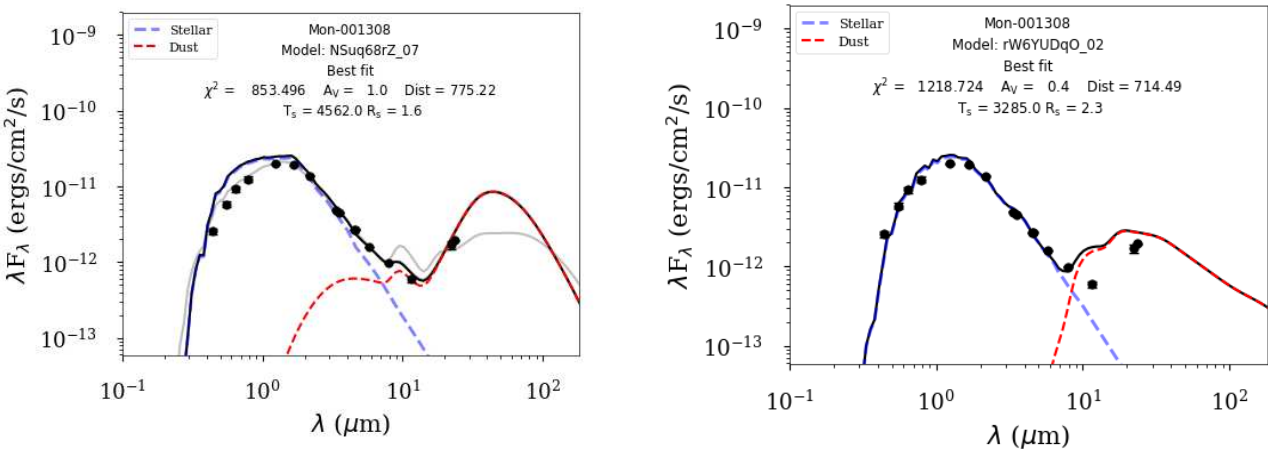


Fig. 1. Two new SED fits for Mon-1308 using the 3D dust continuum radiative transfer code Hyperion. The SED on the left corresponds to the best fit using a stellar photosphere and a full disk. The SED on the right corresponds to the best fit using a stellar photosphere and a disk with an inner hole (TD). The plot includes the values for the fitted parameters. The emission comes from the star (blue line), and a full-disk or TD (red line). The total flux is shown as a black line. The color figure can be viewed online.



uncertainties. The input fluxes use $UBVRcIc$ optical photometry from Rebull et al. (2002), near-IR photometry $JHK$s from 2MASS, *IRAC* (Fazio et al. 2004) and MIPS (Rieke et al. 2004) magnitudes from *Spitzer* satellite, and *WISE* observations at 3.4, 4.6, 12.0, and 22 $\mu$m (Wright et al. 2010). We used the distance estimated from parallax data obtained from the *Gaia* second release (Gaia Collaboration et al. 2016, 2018).

This code does not have a setup for a PTD; thus, we are not able to test this scenario. For the new fit, we remove the SDSS magnitudes because we realized that they are not as trustworthy compared to $UBVRI$ data. The magnitudes are input parameters in the code. Besides, using a different $A_v$ range from Sousa et al. (2019); we find a new fit for the data with a full disk model with more consistent $T_\star$ and inclination $i$ values. Instead of $A_v = 0.2$, $T_\star = 5011$K and $i = 86.4°$, the new values are $A_v = 1$, $T_\star = 4562$K and $i = 60.99°$. We try to fit the observational data using a TD but the $i$ obtained is $i = 18.8°$, a value not consistent with the variability observed in the lcs which requires dusty structures that intermittently block the stellar radiation only present in a high-i configuration. As a secondary argument, against the TD model $\chi^2 = 1218.724$ compared to $\chi^2 = 853.496$ for the full-disk case. Both new fits are shown in Figure 1.

Summarizing, there are three important facts. The first one is that our modeling of the lcs is unsuccessful; thus, the presence of dust in the inner hole (a TD) is not consistent with this part of the observations. The second fact is that the PTD scenario cannot be tested. The third is that the new fitting of the SED suggest that a full disk in Mon-1308 is reasonable. Our conclusion is that a full disk could be a possible option for this object.

### 4.2. *Mon-433*

For both, $\Delta mag_{\rm obs}$ and $\Delta mag_{\rm IR,obs}$, the range is $[0.2, 0.4]$. A fit for $\Delta mag_{\rm obs}$ is not found for the ranges of $\alpha$ and $\beta$ studied ($0.1 < \alpha < 10$,$0 < \beta < 1$). For these models $\Delta mag < 0.1$ which is not consistent with the observations. We require an increase of more than one order of magnitude in $\dot{M}$ or in the dust to gas ratio to explain $\Delta mag_{\rm obs}$, but in any case we are unable to interpret $\Delta mag_{\rm IR,obs}$. The larger observational estimate of $\dot{M}$ is only 1.23 times the value used for the modeling. Thus, the evidence leads us to conclude that the optically thin material in the hole is not enough to interpret the lcs in the optical and in the IR.

In Table 2 we show that the periodicity analysis done in Cody et al. (2014) indicates that there is no clearly defined period for the *CoRoT* lc of Mon-433. This is summarized in McGinnis et al. (2015), where they catalogued the *CoRoT* light curve in 2011 as aperiodic. However, over a timescale of around 5 to 10 days, there is a sequence of peaks and valleys that indicates that underneath it there is some periodic physical structure as the one presented in this work. Around this main periodic structure there

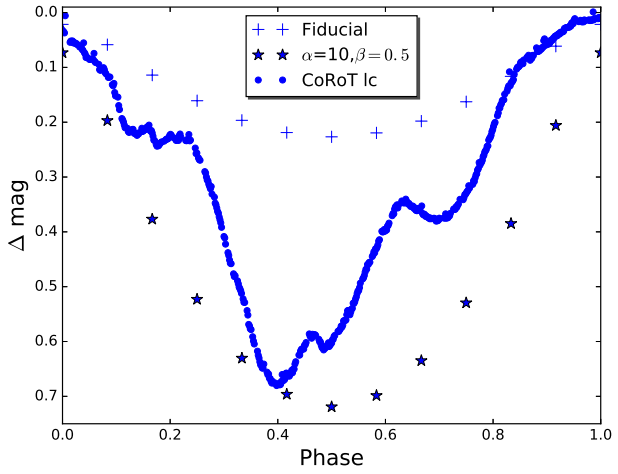


Fig. 2. Two models for the optical lc of Mon-296. The first model is shown with plus signs, corresponding to the fiducial: $\alpha = 1$ and $\beta = 1$. The second model is represented with stars, corresponding to $\alpha = 10$ and $\beta = 0.5$. The points show a representative section of the *CoRoT* lc in the 2011 Campaign. The color figure can be viewed online.

is another set of minor structures located at different places with different periods which shape the observed light curve. This evidence leads us to a physically reasonable test of this model. As in Mon-1308, for Mon-433 a PTD includes a structure responsible to add another component for the extinction in order to explain the observations. We are unable to test this using the SEDfitter code based on Hyperion because it does not have a setup for a PTD, just for full disks and TDs.

### 4.3. *Mon-314*

For both $\Delta mag_{\rm obs}$ and $\Delta mag_{\rm IR,obs}$, the range is $[0.1, 0.15]$. A fit for $\Delta mag_{\rm obs}$ is found when $\alpha = 0.3$ (and $0 < \beta < 0.4$), $\alpha = 0.5$ (and $0.1 < \beta < 0.7$) and $\alpha = 0.7$ (and $0.4 < \beta < 1$). Due to the grid of models, we run models for $\alpha = 0.3, 0.5$ and $0.7$ but not for intermediate values; however, other models with values of $\alpha$ between 0.3 and 0.7 are also inside the range of $\Delta mag_{\rm obs}$. For these models $\Delta mag_{\rm IR} < 10^{-2}$ which is one order of magnitude lower than required for a reasonable fit. The optical flux from the model lies between the $F_{\rm min,opt}$ and $F_{\rm max,opt}$, values given in Table 4. In Table 4 the range of fluxes modeled at 3.6$\mu$m is presented, spanning between $F_{\rm min,IR}$ and $F_{\rm max,IR}$. These values are consistent with the modeling in Sousa et al. (2019). Note that the values for $\alpha$ imply that the dust-to-gas ratio is lower than typical for protoplanetary disks. However, we think that the models are physically reasonable to explain $\Delta mag_{\rm obs}$ but their inability to explain $\Delta mag_{\rm IR,obs}$ led us to look for another configuration.

As the objects Mon-1308 and Mon-433, Mon-314 also satisfy $\Delta mag \approx \Delta mag_{\rm IR}$, the analyses developed in § 4.1 are valid here. Table 4 shows some parameters from the modeling of two cases explaining $\Delta mag_{\rm obs}$.

Note that McGinnis et al. (2015) do not find a stable period in the lc. However, it is clear that the physical mechanism repeats itself, because within a temporal range a sequence of peaks and valleys is clearly seen in the lc. Thus, it is valid to try a periodical model to fit the photometric data. As for Mon-433, a likely model for Mon-314 is a PTD.

### 4.4. *Mon-296*

For $\Delta mag_{\rm obs}$ and $\Delta mag_{\rm IR,obs}$, the range is $[0.2, 0.7]$ and $[0, 0.1]$, respectively. A fit for $\Delta mag_{\rm obs}$ is found when $\alpha = 0.7$ (and $0 < \beta < 0.3$), $\alpha = 1$ (and $0 < \beta < 1$), $\alpha = 3$ (and $0 < \beta < 1$), $\alpha = 5$ (and $0 < \beta < 0.8$), $\alpha = 7$ (and $0 < \beta < 0.7$) and $\alpha = 10$ (and $0 < \beta < 0.5$). Due to the grid of models, we run models for $\alpha = 0.7, 1, 3, 5, 7$ and 10 but not for intermediate values; however other models with values of $\alpha$ between 0.7 and 10 are also inside the range for $\Delta mag_{\rm obs}$. For these models $\Delta mag_{\rm IR}$ is between $1.05 \times 10^{-2}$ and $4.37 \times 10^{-2}$ which is an order of magnitude lower than required for a reasonable fit. The optical flux coming from the model lies between the $F_{\rm min,opt}$ and $F_{\rm max,opt}$, values given in Table 4. These values are consistent with the SED fitting in Sousa et al. (2019).

For Mon-314, Mon-433, and Mon-1308, $\Delta mag_{\rm IR}$ is between two and three orders of magnitude lower than $\Delta mag_{\rm IR,obs}$. For the fiducial model for Mon-296, $\Delta mag = 0.226$ and $\Delta mag_{\rm IR} = 0.01$. This is the only system for which the fiducial model is consistent with $\Delta mag_{\rm obs}$. For a 10 times more massive hole ($\alpha = 10$) with $\beta = 0.5$, both values increase to: $\Delta mag = 0.719$ and $\Delta mag_{\rm IR} = 0.0437$, the last value is consistent with the observed IR lc. The modeled lcs corresponding to the previous cases are presented in Figure 2 for the optical and in Figure 3 for the IR. Also in the figures we include a section of the *CoRoT* and *Spitzer* lcs for Campaign 2011. An increase of the dust abundance and/or $\dot{M}$ is required to explain the lcs within the framework of this modeling. Another possibility is that the material in the hole is not completely thin but coexists with partial or completely optically thick structures, like streams that connect the outer disk with the star.

In Table 4 the ranges of the total flux modeled at 3.6$\mu$m for the fiducial and the massive model are

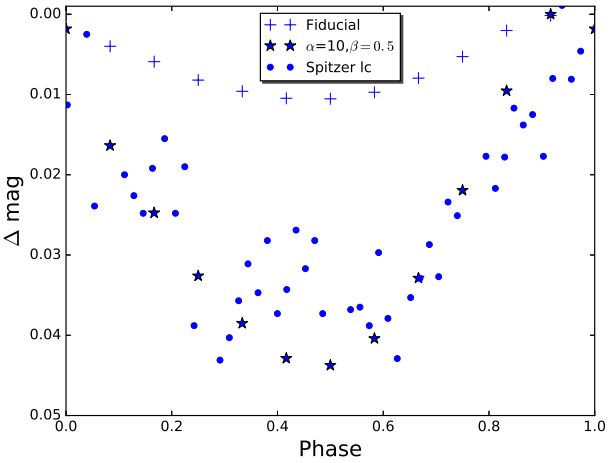


Fig. 3. Two models for the IR lc of Mon-296. The first model is shown with plus signs, corresponding to the fiducial: $\alpha = 1$ and $\beta = 1$. The second model is represented with stars, corresponding to $\alpha = 10$ and $\beta = 0.5$. The points show a representative section of the *Spitzer* lc in the 2011 Campaign. The color figure can be viewed online.

presented, spanning between $F_{\rm min,IR}$ and $F_{\rm max,IR}$. In the models for the optical, the total flux range lies between $F_{\rm min,opt}$ and $F_{\rm max,opt}$. These values are consistent with the modeling in Sousa et al. (2019). If we extract the contribution of the stellar flux in the optical and in the IR then $F_\star \approx 5 \times 10^{-11}$ and $F_{\star,\rm IR} \approx 5 \times 10^{-12}$, which are consistent with the SED presented in Sousa et al. (2019). In the fiducial case, the IR flux of the material in the hole is $F_{\rm IR} \approx 5 \times 10^{-13}$, which is one order of magnitude lower than the flux associated to the optically thick disk required for the modeling using the SED fitting code based in Hyperion (Sousa et al. 2019). However, the hole material for the massive model produces a flux given by $F_{\rm IR} \approx 3.29 \times 10^{-12}$, where $F_{\rm IR}/F_{\star,IR} = 0.7$, just a factor of two lower than the observational estimate of 1.6 for 4.5$\mu$m in McGinnis et al. (2015). The value for $F_{\rm IR}$ is estimated as the excess above the photospheric template used to calculate $F_{\star,\rm IR}$. This means that in the latter case the flux of the material in the hole does noticeably affect the SED fitting. But it is still necessary to explain the lcs in both the optical and the IR.

An estimate of the surface density required to calculate the extinction is done using the constant parameter $A$ in equation 1, such that the largest value corresponds to Mon-296. This explains the existence of many models consistent with $\Delta mag_{\rm obs}$. Also, among our set of objects, this is the only one satisfying $\Delta mag >> \Delta mag_{\rm IR}$, resulting in the emission and occultation caused by a small optically thin hole to be consistent either with the SED as shown in Sousa et al. (2019) or the *CoRoT* and *Spitzer* lcs presented in McGinnis et al. (2015). Note that the optically thick disk outside the hole can produce occultations for inclinations larger than $a\tan(R_{\rm H}/H_{\rm H}) = 84.29°$, meaning that for this object the occultation structure is located inside the hole. For the other objects, occultations caused by the outer edge of the hole are not relevant according to the evidence iof the lcs, namely, the variability timescale is associated to their inner regions.

## 5. DISCUSSION

For Mon-1308, the presence of a small optically thick inner disk is required in order to simultaneously explain the optical and IR lcs, because in this case both lcs have a strong resemblance, and hence the physical region shaping both is the same. As noted in § 4.1, we are able to explain the optical lc with the material concentrated at the inner edge of the disk. However, in order to fit the IR lc, an increase in the amount of dust by several orders of magnitude is required, which is not physically correct.

Because it is not possible to find a physically correct modeling for the optical and IR lcs for Mon-314 and Mon-433, we suggest that these two systems require a small optically thick disk in the innermost regions responsible to shape both lcs. This is consistent with the LkCa 15 TD because it has a 50 AU wide cavity (Andrews et al. 2011b), and also a photometric variability with a very small period, which implies a disk-like structure located very close to the star (Alencar et al. 2018).

For Mon-296, the $R_{\rm k}$ consistent with the stellar rotational period $P$ is less than $R_{\rm H}$; thus the material responsible to shape the periodic optical lc is inside the optically thin environment. For this object, $R_{\rm k} = 0.054$ AU and $R_{\rm H} = 0.12$ AU, such that $R_{\rm ovr} = 0.086$ AU is inside this range. $R_{\rm ovr}$ is the location of the outer vertical resonance, which results from the analysis of the propagation of small-amplitude waves in the disk. Here, the study of out-of-plane gravity modes implies the excitation at this radius of bending waves. This analysis results from the linearization of the equations of motion for the fluid in the disk, where the external force is calculated with the stellar magnetic field, which is moving at the stellar rotational velocity (Romanova et al. 2013). The bending wave rotates at the stellar rotational velocity. Thus it is a structure likely to explain periodicity with the period corresponding to this velocity. Note that a value of $\beta = 0.9$ means that 66% of the material is moving at the velocity required

to have a periodic feature with a period $P$. However, the model explaining $\Delta mag_{\rm obs}$ corresponds to $\beta = 0.5$ implying that not all the dust is distributed in a region where the material is rotating with period $P$. It is important to mention that the modeled optical and IR lcs evolve with the same periodicity, but for Mon-296 there is no clear resemblance between the observed lcs. This leads to an interpretation where the actual dust distribution is not completely described by the density $\rho$ given in equation 1. This $\rho$ works as the backbone of the actual structure, where the multiple features expected in a highly dynamical environment near the stellar magnetosphere are important to explain the details of the lcs.

Optically thin dust emission does not depend on the lc phase; thus, the low amplitude magnitude shown in the *Spitzer* lc for Mon-296 is consistent with this fact; note that at many different times the IR magnitude is constant. The small value for $R_H$ means that an optically thick disk is close enough to the star to have an adequate temperature to contribute in the IR, as can be seen in Sousa et al. (2019). This is important because the physical configuration for the model presented here results in similar shapes for the optical and IR lcs, which is contrary to the observations. Thus, we can argue that an optically thick disk flux contribution changing with phase is relevant as a second mechanism to fully interpret the IR variability.

## 6. CONCLUSIONS

1.- For Mon-314 and Mon-1308, $\Delta mag \approx \Delta mag_{\rm IR}$ but the model predicts $\Delta mag >> \Delta mag_{\rm IR}$. Thus, we are able to model $\Delta mag_{\rm obs}$ but not to consistently model $\Delta mag_{\rm IR,obs}$. Using the grid of models defined within the range $0.1 < \alpha < 10$ and $0 < \beta < 1$, we cannot find a consistent model for Mon-433. Mon-296 is the only system where $\Delta mag >> \Delta mag_{\rm IR}$; hence this is the only object that can be modeled using the optically thin material inside the disk.

2.- The density in a small optically thin hole (≈tenths of AU) is large enough to explain typical amplitudes (≈tenths) of the optical lc produced by dust extinction of the stellar spectrum. Using the observed stellar and disk parameters, Mon-296 can be explained with the fiducial model ($\alpha = 1$ and $\beta = 1$). This value of $\beta$ corresponds to material concentrated at the inner edge of the hole, a fact consistent with the small period of the variability, which locates the extinct material very close to the star.

3.- Neither the extinction in the IR caused by the hole material nor the stellar occultations contribute noticeably to $\Delta mag_{\rm IR}$, ending with a very low value. Note that as $R_{\rm H}$ increases, the fraction of material occulted by the star decreases, and therefore its contribution to $\Delta mag_{\rm IR}$ also decreases. Thus, Mon-296 is the object that contributes the most to $\Delta mag_{\rm IR}$, as can be seen in the modeling.

4.- The extinction is given by the surface density along the line of sight. The largest value corresponds to Mon-296, resulting in the largest contribution to $\Delta mag_{\rm IR}$. Thus, along with the smallest $R_{\rm H}$ as mentioned in the previous item, both facts lead to the largest non-negligible value of $\Delta mag_{\rm IR}$ for Mon-296.

5.- According to the modeling, Mon-314, and Mon-433 require an optically thick inner disk to interpret the lcs. We suggest that instead of hosting a TD they host a PTD. The existence of this structure helps to increase the magnitude amplitude for the IR lcs, as required to interpret the observations. In order to pursue this idea, SED modeling presented by Sousa et al. (2019) should include a small optically thick inner disk. Note that a disk of small size is enough to produce the occultations required to explain $\Delta mag_{\rm obs}$ without noticeably changing the fitting by Sousa et al. (2019).

6.- Using the tool Sedfitter based on Hyperion, a new SED fitting is found for Mon-1308. The new fit favors a full-disk instead of a TD. This is consistent with the modeling of the lcs by Nagel & Bouvier (2019) and with our inability to explain the lcs using optically thin material in the hole. We do not have the tools to test the PTD scenario, but it is also a possible scenario for Mon 1308. Our final remark is that we cannot rely on a SED fitting alone. An analysis of lcs in the optical and in the IR may give us relevant information to cast doubt on this preliminary result. Indeed, revisiting Mon-1308 led us to conclude that the most probable configuration for this object is a full-disk.

## REFERENCES

Alencar, S. H. P., Teixeira, P. S., Guimarães, M. M., et al. 2010, A&A, 519, 88, DOI: 10.1051/0004-6361/201014184

Alencar, S. H. P., Bouvier, J., Donati, J.-F., et al. 2018, A&A, 620, 195, DOI: 10.1051/004-6361/201834263

Andrews, S. M., Wilner, D. J., Espaillat, C., et al. 2011, ApJ, 732, 42, DOI: 10.1088/0004-637X/732/1/42

Andrews, S. M., Rosenfeld, K. A., Wilner, D. J., & Bremer, M. 2011, ApJ, 742, 5, DOI: 10.1088/2041-8205/742/1/L5

Ansdell, M., Gaidos, E., Rappaport, S. A., et al. 2016, ApJ, 816, 69, DOI: 10.3847/0004-637X/816/2/69

Blinova, A. A., Romanova, M. M., & Lovelace, R. V. E. 2016, MNRAS, 459, 2354, DOI: 10.1093/mnras/stw786

Bodman, E. H. L., Quillen, A. C., Ansdell, M., et al. 2017, MNRAS, 470, 202, DOI: 10.1093/mnras/stx1034

Bouvier, J., Chelli, A., Allain, S., et al. 1999, A&A, 349, 619

Bouvier, J., Grankin, K., Ellerbroek, L. E., Bouy, H., & Barrado,D. 2013, A&A, 557, 77, DOI: 10.1051/004-6361/201321389

Calvet, N., D'Alessio, P., Watson, D. M., et al. 2005, ApJ, 630, 185, DOI: 10.1086/491652

Cieza, L. A., Schreiber, M. R., Romero, G. A., et al. 2010, ApJ, 712, 925, DOI: 10.1088/0004-637X/712/2/925

Cody, A. M., Stauffer, J., Baglin, A., et al. 2014, AJ, 147, 82, DOI: 10.1088/0004-6256/147/4/82
Dullemond, C. P., & Monnier, J. D. 2010, ARA&A, 48, 205, DOI: 10.1146/annurev-astro-081309-130932
Espaillat, C., Calvet, N., D'Alessio, P., et al. 2007, ApJ, 670, 135, DOI: 10.1086/524360
Espaillat, C., Muzerolle, J., Hernández, J., et al. 2008, ApJ, 689, 145, DOI: 10.1086/595869
Espaillat, C., D'Alessio, P., Hernández, J., et al. 2010, ApJ, 717, 441, DOI: 10.1088/0004-637X/717/1/441
Espaillat, C., Furlan, E., D'Alessio, P., et al. 2011, ApJ, 728, 49, DOI: 10.1088/0004-637X/728/1/49
Espaillat, C., Muzerolle, J., Najita, J., et al. 2014, in Protostars and Planets VI, ed. H. Beuther, R. S. Klessen, C. P. Dullemond, & T. Henning (Tuczon, AZ: UAP), 497, DOI: 10.2458/azu_uapress_9780816531240-ch022
Fang, M., van Boekel, R., Wang, W., et al. 2009, A&A, 504, 461, DOI: 10.1051/0004-6361/200912468
Fazio, G. G., Hora, J. L., Allen, L. E., et al. 2004, ApJS, 154, 10, DOI: 10.1086/422843
Flaherty, K. M., Muzerolle, J., Rieke, G., et al. 2012, ApJ, 748, 71, DOI: 10.1088/0004-637X/748/1/71
Gaia Collaboration, et al. 2016, A&A, 595, 1, DOI: 10.1051/004-6361/201629272
Gaia Collaboration, et al. 2018, A&A, 616, 1, DOI: 10.1051/004-6361/201833051
Ingleby, L., Espaillat, C., Calvet, N., et al. 2015, ApJ, 805, 149, DOI: 10.1088/0004-637X/805/2/149
Kulkarni, A. K., & Romanova, M. M. 2008, MNRAS, 386, 673, DOI: 10.1111/j.1365-2966.2008.13094
Lovelace, R. V. E., & Romanova, M. M. 2014, FIDyR, 46, 1401, DOI: 10.1088/0169-5983/46/4/041401
Manara, C. F., Testi, L., Natta, A., et al. 2014, A&A, 568, 18, DOI: 10.1051/0004-6361/201323318
Manara, C. F., Rosotti, G., Testi, L., et al. 2016, A&A, 591, 3, DOI: 10.1051/0004-6361/201628549
McGinnis, P. T., Alencar, S. H. P., Guimarães, M. M., et al. 2015, A&A, 577, 11, DOI: 10.1051/0004-6361/201425475
McQuillan, A., Aigrain, S., & Mazeh, T. 2013, MNRAS, 432, 1203, DOI: 10.1093/mnras/stt536
Meheut, H., Casse, F., Varniere, P., & Tagger, M. 2010, A&A, 516, 31, DOI: 10.1051/0004-6361/201014000
Merín, B., Brown, J. M., Oliveira, I., et al. 2010, ApJ, 718, 1200, DOI: 10.1088/0004-637X/718/2/1200
Morales-Calderón, M., Stauffer, J. R., Hillenbrand, L. A., et al. 2011, ApJ, 733, 50, DOI: 10.1088/0004-637X/733/1/50
Muto, T., Grady, C. A., Hashimoto, J., et al. 2012, ApJ, 748, 22, DOI: 10.1088/2041-8205/748/2/L22
Muzerolle, J., Allen, L. E., Megeath, S. T., Hernández, J. & Gutermuth, R. A. 2010, ApJ, 708, 1107, DOI: 10.1088/0004-637X/708/2/1107
Nagel, E., álvarez-Meraz, R., & Rendón, F. 2017, RMxAA, 53, 227
Nagel, E. & Bouvier, J. 2019, A&A, 625, 45, DOI: 10.1051/004-6361/201833979
_____. 2020, A&A, 643, 157, DOI: 10.1051/0004-6361/202038594
Najita, J. R., Strom, S. E., & Muzerolle, J. 2007, MNRAS, 378, 369, DOI: 10.1111/j.1365-2966.2007.11793.x
Najita, J. R., Andrews, S. M., & Muzerolle, J. 2015, MNRAS, 450, 3559, DOI: 10.1093/mnras/stv839
Owen, J. E. & Clarke, C. J. 2012, MNRAS, 426, 96, DOI: 10.111/j.1745-3933.2012.01334.x
Rebull, L. M., Makidon, R. B., Strom, S. E., et al. 2002, AJ, 123, 1528, DOI: 10.1086/338904
Rieke, G. H., Young, E. T., Engelbracht, C. W., et al. 2004, ApJS, 154, 25, DOI: 10.1086/422717
Robitaille, T. P. 2011, A&A, 536, 79, DOI: 10.1051/0004-6361/201117150
_____. 2017, A&A, 600, 11, DOI: 10.1051/0004-6361/201425486
Rodríguez, J. E., Ansdell, M., Oelkers, R. J., et al. 2017, ApJ, 848, 97, DOI: 10.3847/1538-4357/aa8c78
Romanova, M. M., Ustyugova, G. V., Koldova, A. V., & Lovelace, R. V. E. 2013, MNRAS, 430, 699, DOI: 10.1093/mnras/sts670
Sousa, A. P., Alencar, S. H. P., Rebull, L. M., et al. 2019, A&A, 629, 67, DOI: 10.1051/0004-6361/201935563
Stauffer, J., Cody, A. M., Baglin, A., et al. 2014, AJ, 147, 83, DOI: 10.1088/0004-6256/147/4/83
Stauffer, J., Cody, A. M., McGinnis, P., et al. 2015, AJ, 149, 130, DOI: 10.1088/0004-6256/149/4/130
Stauffer, J., Cody, A. M., Rebull, L., et al. 2016, AJ, 151, 60, DOI: 10.3847/0004-6256/151/3160
Sung, H., Stauffer, J. R., & Bessell, M. S. 2009, AJ, 138, 1116, DOI: 10.1088/0004-6256/138/4/1116
van der Marel, N., Cazzoletti, P., Pinilla, P., & Garufi, A. 2016, ApJ, 832, 178, DOI: 10.3847/0004-637X/832/2/178
van der Marel, N., Williams, J. P., Ansdell, M., et al. 2018, ApJ, 854, 177, DOI: 10.3847/1538-4357/aaaa6b
Venuti, L., Bouvier, J., Flaccomio, E., et al. 2014, A&A, 570, 82, DOI: 10.1051/0004-6361/201423776
Wright, E. L., Eisenhardt, P. R. M., Mainzer, A. K., et al. 2010, AJ, 140, 1868, DOI: 10.1088/0004-6256/140/6/1868

Fernando Gutiérrez-Canales, Sebastián Morales-Gutiérrez, and Erick Nagel: Departamento de Astronomía, Universidad de Guanajuato, Callejón de Jalisco S/N, 36240 Guanajuato, Guanajuato, México (e.nagel@ugto.mx).
Alana P. Sousa: Université Grenoble Alpes, IPAG, F-38000 Grenoble, France.